The LINNEAN SOCIETY of London BIOLOGICAL Journal of the Linnean Society

Biological Journal of the Linnean Society, 2016, **118**, 648–667. With 7 figures.

Phylogenetic relationships among species of the Neotropical genus *Graomys* (Rodentia: Cricetidae): contrasting patterns of skull morphometric variation and genetic divergence

JUAN J. MARTÍNEZ[1]* and CRISTINA N. GARDENAL[2]

[1]*Centro de Investigaciones y Transferencia de Jujuy (CIT-Jujuy), CONICET and Universidad Nacional de Jujuy, Av. Bolivia 1711, San Salvador de Jujuy, Jujuy, 4600, Argentina*
[2]*Instituto de Diversidad y Ecología Animal (IDEA), CONICET and Universidad Nacional de Córdoba, Av. Vélez Sarsfield 299, Córdoba, Córdoba, 5000, Argentina*

Received 14 October 2015; revised 2 December 2015; accepted for publication 3 December 2015

Subtle differences of external traits characterize species of rodents in the Neotropical genus *Graomys*. On the other hand, the species differ markedly in chromosome number. In the present study, we evaluate the possible evolutionary forces involved in the evolution of the genus by assessing the degree of intra- and interspecific genetic and morphological variation. A phylogenetic analysis demonstrates the existence of at least three species with high levels of genetic distance (10%), which diverged between 1 and 1.5 Mya. Neither *Graomys griseoflavus*, nor *Graomys chacoensis* present marked phylogeographical structure. Regarding morphological characters, these species show shape differences in the skull that could be attributable to differences in the local conditions they inhabit, being more marked in *G. griseoflavus* than in *G. chacoensis*. The skull shape of *G. chacoensis* could have evolved under genetic drift, whereas evidence reported in the present study indicates that this character could be under selective pressures in *G. griseoflavus*. Reconstruction of the ancestral area suggests that *G. griseoflavus* originated in the central Monte desert, whereas *G. chacoensis* originated in the Chaco ecoregion surrounding the austral extreme of the Yungas rainforest. Subsequently, both species would have undergone demographic and geographical expansions almost simultaneously, starting approximately 150 000–175 000 years ago. The complex evolutionary history of the genus could be partly explained by the decoupling of morphological, karyological and molecular traits. © 2016 The Linnean Society of London, *Biological Journal of the Linnean Society*, 2016, **118**, 648–667.

KEYWORDS: interspecific variation – intraspecific variation – molecular systematics – phylogeography – Sigmodontinae – skull geometric morphometrics – species boundaries.

INTRODUCTION

Determining why phenotypic and genetic differentiation are uncoupled among species and populations is crucial for understanding the causative roles of selection and neutral processes in microevolution. Several sources of evidence must be considered in an integrative systematic approach. Thus, phylogenetic analyses of morphological and DNA sequence data, comparative analyses of multivariate patterns of covariation, analysis of geographical variation, and alpha systematics all comprise an attempt to bridge the micro- and macro-evolutionary scales and understand large-scale patterns.

Schluter (1996) defined a 'line of least evolutionary resistance' as the main direction of intrapopulation variance that can be estimated by the direction of greatest genetic variance (G_{max}), which corresponds to the major axis of genetic variance/covariance (V/CV) matrices (Steppan, Phillips & Houle, 2002; McGuigan, Chenoweth & Blows, 2005). The study of the main direction of variance provides a conceptual and methodological framework for bridging the gap between different evolutionary scales. Variation

*Corresponding author. E-mail: juan_jmart@yahoo.com.ar

estimated at the intrapopulation level can be compared with long-term evolutionary trajectories at the species level. This approach allows possible developmental constraints on phenotypic evolution to be inferred (Renaud & Auffray, 2013).

By contrast, the analysis of genetic variation by means of phylogeography allows inferences to be made about selection, population structure, and demographic changes based on neutrality tests and coalescence. This approach helps to clarify the evolutionary determinants of genetic variation, as well as the relationships between genetic and phenotypic differentiation. The data obtained contribute greatly to taxonomic revisions, including the detection of sibling species and the 'lumping' of species with fuzzy boundaries as a result of morphological similarity (Granjon & Montgelard, 2012).

To contribute to our understanding of the process of diversification in the genus *Graomys* (Cricetidae, Sigmodontinae), we applied an integrative analysis of morphometric, ecogeographical, and genetic variation at intraspecific levels to explain its evolutionary history. The genus *Graomys* includes four extant species of medium-sized rodents, mainly distributed in southern Neotropical region: *Graomys chacoensis*, *Graomys domorum*, *Graomys edithae*, and *Graomys griseoflavus*. *Graomys edithae* is maintained as valid but waiting for further evidence because nothing is known beyond its original description. These rodents inhabit a great variety of ecoregions, such as Chaco forests and savannas, Monte desert, transitional forest of the Yungas, and Patagonian steppes (Anderson, 1997; Díaz *et al.*, 2006). At present, *Graomys* is recognized as a genus of full rank based on morphological and cytogenetic studies (Pearson, 1972; Wainberg & Fronza, 1974; Pearson & Patton, 1976; Olds & Anderson, 1989) and recent molecular evidence (Anderson & Yates, 2000; Steppan *et al.*, 2007). However, most of the studies are based only on cytochrome *b* (*mt-cyb*) sequences, with results about interspecific relationships in the genus remaining nonconclusive (Catanesi *et al.*, 2002; Steppan *et al.*, 2007).

Until recently, populations of *G. griseoflavus* and *G. chacoensis* were considered to belong to the same species, under the name of *G. griseoflavus* (Theiler & Blanco, 1996b; Catanesi *et al.*, 2002; Ferro & Martínez, 2009). This was supported by two main observations: the high external morphological and skull morphometric similarity between these species (Martínez & Di Cola, 2011) and the existence of intrapopulation chromosomal polymorphisms ($2n$ = 33–38 and 41–42) originating from Robertsonian or centric fusions (Wainberg & Fronza, 1974; Zambelli, Vidal-Rioja & Wainberg, 1994; Lanzone *et al.*, 2014). Cytogenetics, reproductive behaviour, and gonadal histology derived from inter-cytotype crosses were performed in populations from central-western Argentina, confirming that specimens with $2n$ = 42 deserve a taxonomic distinction at the species level. Theiler & Blanco (1996a) also noted prezygotic isolation between the species, which involved olfactory discrimination of interspecific males by females, preventing nonviable descendants of sterile hybrids. Ecogeographical segregation between those species was later highlighted: *G. griseoflavus* occurs mainly in desert ecoregions such as the Monte desert and Patagonian steppe, whereas the form referred to as *G. chacoensis* occurs mainly in the Dry Chaco and the Espinal forests (Theiler, Gardenal & Blanco, 1999; Díaz *et al.*, 2006; Ferro & Martínez, 2009; Martínez & Di Cola, 2011).

In the present study, we assessed phylogenetic relationships and species boundaries using both multilocus molecular and morphometric approaches. In addition, we incorporated an ecogeographical analysis of genetic and morphometric variation. We estimated the times of divergence within the genus and the location of ancestral areas. In the morphometric analysis, we include holotype specimens of *G. edithae*, *G. chacoensis*, *Graomys lockwoodi*, and *Graomys cachinus*, whose present taxonomic status is controversial. The species of the genus would have diverged as a result of a complex process, with morphological, genetic, and cytogenetic traits following different trajectories and tempos of evolution.

MATERIAL AND METHODS

Molecular analysis

Tissue samples for DNA extraction were obtained both from specimens housed in museum collections and from animals collected during field trips. In total, 50 *Graomys* specimens were sequenced, including topotypic specimens from Chumbicha (*Graomys medius* junior synonymous of *G. chacoensis*) and one specimen of *G. domorum* captured in Argentina (locality 2 in Fig. 1). Additionally, 34 sequences of *mt-cyb* were obtained from the GenBank database (see Supporting information, Table S1). Detailed information about specimens and localities is provided in the Supporting information (Table S1) and Figure 1.

Phylogenetic inference and dating

Total genomic DNA was extracted using the method described for ethanol-preserved tissues in accordance with the standard salt extraction method (Bruford *et al.*, 1992), precipitated in absolute ethanol, dried, and stored in Tris buffer (Tris-EDTA) pH 8. The *mt-cyb* sequences were obtained in accordance with the

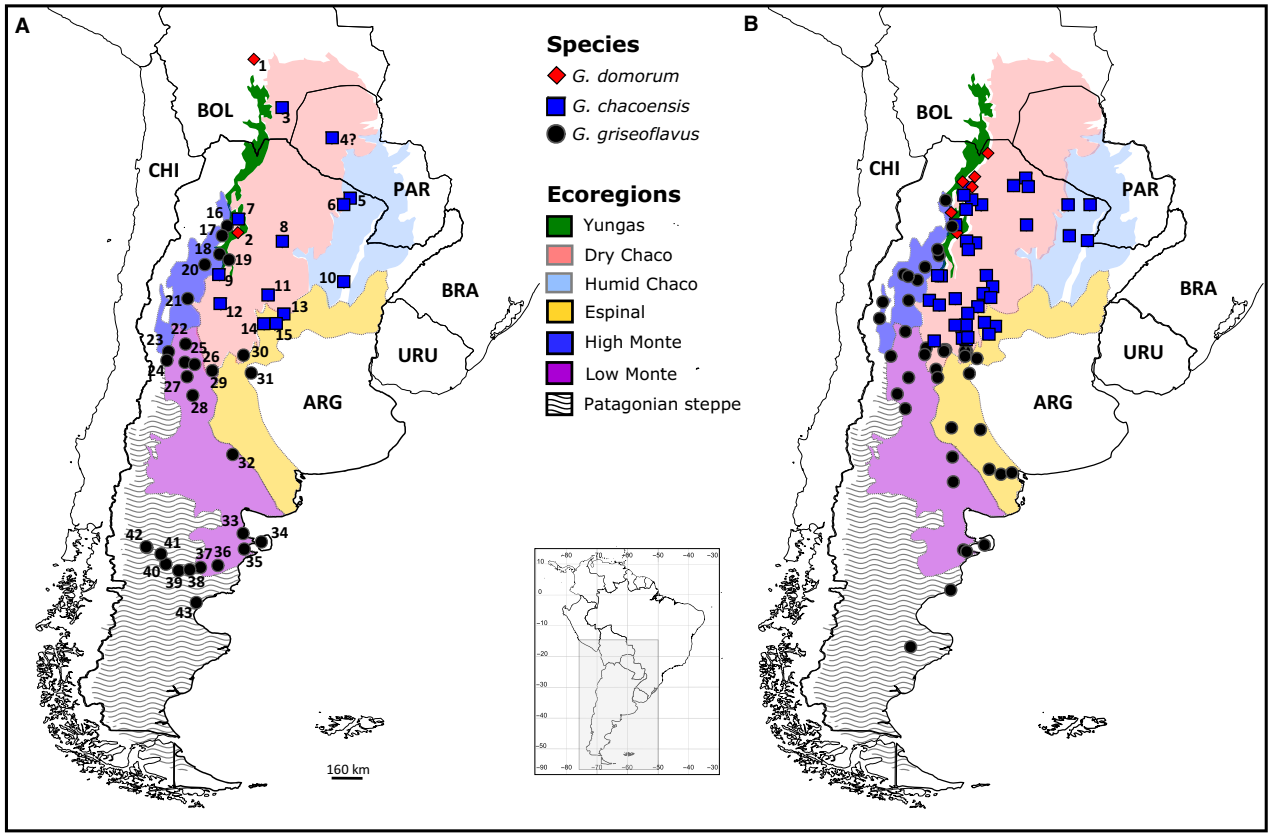

Figure 1. Sampling location of *Graomys* according to ecoregions in southern South America. A, the localities of *Graomys* specimens used in *mt-cyb* phylogeography analysis. B, the localities of *Graomys* specimens used in skull morphometric analyses. The localities are detailed in the Supporting information (Appendix S1). ARG, Argentina; BRA, Brazil; BOL, Bolivia; CHI, Chile; PAR, Paraguay; URU, Uruguay.

protocol described in Ferro & Martínez (2009) using primers Mus14095, Mus15398, and Mvz16 (da Silva & Patton, 1993; Anderson & Yates, 2000) (see Supporting information, Table S2). To estimate species relationships, we incorporated additional molecular markers (see Supporting information, Table S2): two nuclear (IRBP and RAG1) and two mitochondrial (control region and ND3). The control region was amplified as described in Martínez *et al.* (2010) using F1 and R2 primers. We amplified ND3 using the same protocol outlined in Kennedy & Nachman (1998) and, for the nuclear segments, we followed Martínez *et al.* (2012) and Steppan *et al.* (2007) for IRBP and RAG1, respectively. Polymerase chain reaction products were purified and sequenced by Macrogen (www.macrogenusa.com) and deposited in GenBank. In total, 84 *mt-cyb* sequences were used in the analyses. Detailed information about voucher and localities is provided in the Supporting information (Appendix S1).

Sequences from other genera were incorporated to infer the relationships of species of *Graomys* in the context of Phyllotini diversification (Table 1). All trees were rooted using *Delomys sublineatus*, based on previous results (Martínez *et al.*, 2012; Parada *et al.*, 2013; Salazar-Bravo, Pardiñas & D'Elía, 2013). Sequence data sets were aligned independently using default parameters of the multiple alignment algorithm implemented in MUSCLE, version 3.6 (Edgard, 2004). We analyzed all of the phylogenetic relationships among *Graomys* species and close relatives using two methods: Bayesian inference was performed with MrBayes, version 3.3 (Ronquist & Huelsenbeck, 2003) and TNT software was used for parsimony inference (Goloboff, Farris & Nixon, 2008). We performed several analyses using: (1) *mt-cyb* dataset (1143 bp); (2) mitochondrial dataset (*mt-cyb*, ND3 and control region) (3076 bp); (3) nuclear markers (IRBP and RAG1) (2632 bp); and (4) the five markers (5708 bp).

For the *mt-cyb* dataset, the model HKY + G + I was selected in accordance with Akaike information criterion (AIC), which was performed in JMODELTEST, version 2.1.3 (Darriba *et al.*, 2012). For

Table 1. List of Phyllotini species and *Graomys* specimens used for phylogenetic inferences

Species/specimen	*mt-cyb*	ND3	*D-loop*	RAG1	IRBP
Delomys sublineatus	AF108687				AY163582
Calassomys apicalis	JQ434425				JQ434417
Calomys callosus	AY275113	U83819	AY033222		AY277440
Calomys laucha	AY033190	U83818	AY033227	AY963173	JQ434404
Calomys lepidus	EU579473				AY163580
Calomys hummelincki	AF385598				JQ434403
Calomys sorellus	AF385608				JQ434406
Calomys tener	DQ447302				JQ434407
Calomys venustus	AY033174		AY033212	AY963174	JQ434408
Calomys musculinus	AF385599	U83817	DQ029212	AY963175	JQ434405
Eligmodontia typus	AF108692	U83816			AY277445
Eligmodontia morgani	EU377631				
Eligmodontia puerulus	EU377652				
Eligmodontia bolsonensis	EU377655				
Eligmodontia moreni	EU377654				
Eligmodontia hirtipes	EU377636				
Salinomys delicatus	EU377608				JQ434415
Andalgalomys pearsoni	JQ434418			AY963176	JQ434398
Galenomys garleppi	JQ434423				JQ434410
Loxodontomys micropus	AY275122			AY963183	JQ434412
Auliscomys sublimis	JQ434421			AY963182	JQ434402
Auliscomys pictus	U03545				JQ434401
Auliscomys boliviensis	JQ434420				JQ434400
Tapecomys primus	AF159287				JQ434416
Tapecomys wolffsohni	AY956698			AY963185	
Phyllotis xanthopygus	AY275128			AY963238	AY277471
Phyllotis darwini	AY956729	U83815	JN226688	AY963223	
Phyllotis osilae	U86829			AY963190	
Graomys griseoflavus (LIF922)	KC699970	KC699987	KC699983	KC699998	KC699993
Graomys griseoflavus (CL99)	KC699981			KC699994	
Graomys griseoflavus (UP278)	AY275117			AY963179	AY277449
Graomys griseoflavus (GRT004)	KC699984	KC699988	KC699984	KC699999	
Graomys domorum (MSB55291)	AF159291			AY963178	
Graomys domorum (LIF914)	KC699945	KC699990	KC699985	KC699996	KC699991
Graomys chacoensis (LIF916)	KC699937	KC699989	KC699986	KC699997	KC699992
Graomys chacoensis (TK65617)	EU579472				EU649037
Graomys chacoensis (CL125)	KC699942			KC699995	

The GenBank accession number is given for each molecular marker when applicable.

Bayesian inference, we used two starting trees with four Markov chain Monte Carlo simulations (three hot and one cold), each one during 30 million generations, with sampling every 1000 generations. The first 5000 trees were discarded as burn-in and the remaining trees were resumed in a 50% majority rule consensus tree. Posterior probabilities were used as node support. The convergence was evaluated using several diagnostic parameters: effective sample size > 500 for several parameters, SD of split frequencies and potential scale reduction factor. For the remaining data sets (mitochondrial, nuclear and total), the best evolutionary models according to AIC were: GTR + G + I for ND3; HKY + G for the control region and IRBP; and, finally, HKY + I for RAG1. The Bayesian inference consisted of Markov chain Monte Carlo simulations run for 15 million generations; two starting trees were used to estimate the convergence in the chains, which consisted of four chains (one cold and three hot). The trees were sampled every 1000 generations. At the end of the analyses, the first 25% of the resulting trees were discarded as burn-in, whereas the remaining trees were used to construct 50% majority-rule consensus phylograms. Convergence was assessed as described above.

Parsimony analysis of *mt-cyb* data set was performed with all sites weighted equally and gaps treated as missing characters. We employed the New Technology approach (Goloboff, 1999; Goloboff *et al.*, 2008); we performed a driven search with 100 random addition sequences using 'ratchet', 'sectorial search', 'drift', and 'tree fusing' as algorithms. The minimum length trees were resumed in a strict consensus tree. For the mitochondrial, nuclear, and total evidence data sets, the maximum parsimony analyses consisted of heuristic searches of 300 random-addition sequences, keeping five trees per replicate and tree bisection and reconnection branch swapping after the random addition sequences. The node supports were evaluated by performing 1000 replicates of bootstrap and jackknife (removal probability 0.36) resampling methods (Felsenstein, 1985; Farris *et al.*, 1996). Character states were equally weighted and gaps were treated as missing.

The *mt-cyb* genetic distances within and between species were estimated using the Kimura two-parameter distance to correct for multiple hits, as implemented in MEGA, version 5 (Kumar *et al.*, 2008). Standard errors were calculated using the bootstrap method with 1000 replicates.

To test whether the species *G. griseoflavus* and *G. chacoensis* experienced either selection or demographic changes, we calculated Fu's F_S (Fu, 1997) and Tajima's *D* (Tajima, 1989), and performed mismatch distribution (Rogers & Harpending, 1992) analyses for *mt-cyb* sequences in ARLEQUIN, version 3.5 (Excoffier & Lischer, 2010). We conducted a Bayesian skyline plot (BSP) analyses (Drummond *et al.*, 2005) using BEAST, version 1.8 (Drummond & Rambaut, 2007) to determine the age of these demographic expansions. This coalescent-based method estimates the effective population size (N_e) over time with an algorithm that takes into account both the error inherent in phylogenetic reconstruction and the stochastic error intrinsic to the coalescent process. We employed the model HKY + G + I for the *mt-cyb* dataset. The analyses, one for each species, were run for 30 million generations; the rate of substitution used was 2.38% Myr^{-1}, according to the rate of divergence obtained for Phyllotini phylogenetic date of divergence (see below). The chain convergences, the estimations of effective population size and confidence intervals for each parameter, and BSP reconstructions were performed using TRACER (Rambaut & Drummond, 2003).

Genetic differentiation among the three species of *Graomys* was tested using a hierarchical analysis of molecular variance (AMOVA) (Excoffier, Smouse & Quattro, 1992) as performed in ARLEQUIN, version 3.5. To estimate among-population genetic divergence within *G. chacoensis* and within *G. griseoflavus*, we performed two AMOVA analyses, one for each species. In total, 10 000 permutations were used to test the significance of variance components and fixation indices.

Bayesian analysis was performed on the total dataset using BEAST, version 1.8 (Drummond *et al.*, 2006; Drummond & Rambaut, 2007) to estimate the dates of divergence on the major lineages of Phyllotini and within *Graomys*. The posterior probability distributions of age nodes were obtained with the five markers, taking into account the previously described molecular models. Two independent analyses (of two runs each) using two different calibration points (see below for details) were implemented assuming a birth–death speciation process and log-normal, uncorrelated rates of variation through branch trees under a relaxed clock model (Drummond *et al.*, 2006). The estimates were obtained by sampling every 1000 MCMC generations from a total of 15 000 000 (15 000 generations were considered as burn-in). The results of MCMC analysis were examined with TRACER, version 1.5 (Rambaut & Drummond, 2003), which suggested adequate sampling, because the parameters of interest always had an EES value higher than 500. After inspecting for convergence on the posterior distributions and reaching the stationary phase of the two runs, we discarded the burn-in period of the sampled trees and combined them into a single tree data file using LOGCOMBINER (Drummond *et al.*, 2012). TREEANNOTATOR (Drummond *et al.*, 2012) was used to summarize the topology with the best support, calculating the maximum clade credibility tree and 95% credible intervals for the node ages.

As noted above, we used two different calibration points: one based on the fossil record and the other based on a previous analysis of the date of divergence for the major groups of the Sigmodontinae radiation (Parada *et al.*, 2013). For the first approach, we used the fossil record of *Auliscomys formosus* to calibrate the crown of Phyllotini (Pardiñas & Tonni, 1998; Smith & Patton, 1999; Parada *et al.*, 2013). We implemented this calibration using a log-normal prior distribution with a mean of 0.01 and SD of 0.6. The calibration was implemented as: the offset = 4.95 (Mya), the median = 5.96, the 5% quantile = 5.326, and the 95% quantile = 7.66. The 5% quantile represents the minimum age of the fossil and the 95% quantile represents both the uncertainty of the fossil age and the incompleteness of the fossil record. According to Parada *et al.* (2013), the Phyllotini diverged 6.93 ± 0.01 Mya (mean ± SD). We implemented these values using a normal prior distribution, typically used when a secondary calibration from a previous study is available.

Estimation of ancestral areas

To assess the geographical locations of the most recent common ancestor of *G. griseoflavus* and *G. chacoensis*, we used PHYLOMAPPER, version 1 (Lemmon & Lemmon, 2008). This method implements a model of migration in a continuous landscape and uses spatial data (i.e. locality geographical coordinates) combined with a rooted genealogy to estimate the coordinates of ancestors under a Bayesian approach. Under this framework, it calculates the likelihood of observing the tips of the tree at their current geographical locations, given the geographical coordinates of clade ancestors and the dispersal distance of the species (Lemmon & Lemmon, 2008).

The analyses were carried out on the *mt-cyb* dataset using a default setting of 10 replicates of smoothing and 100 replicates for optimization after setting the focal clade (i.e. clades of *G. griseoflavus* and *G. chacoensis*, respectively). Both parameters require replicates to be run in the analysis because the nonparametric rate smoothing procedure uses a hill-climbing approach and entrapment in a local optimum is feasible. We replicated our analysis in PHYLOMAPPER 100 times for each species to take phylogenetic uncertainty into account. Thus, we selected 100 random trees from the after-burn-in samples of Bayesian inference based on 84 sequences of *mt-cyb* belonging to specimens of *Graomys* plus two outgroup sequences: *Calomys musculinus* and *Calomys venustus*. Those 100 ancestral coordinates for each species were used to create a minimum convex polygon area of 95%.

Specimens and morphometric protocol

We digitized 11 and 14 landmarks in dorsal (273 specimens) and ventral views (262 specimens) of the skull, respectively (Fig. 2; Table 2). The adult specimens come from an area that covers most of the species distribution in Argentina (Fig. 1), and they include the holotypes of *G. edithae*, *G. cachinus*, *G. lockwoodi*, and *G. chacoensis* from the British Museum of Natural History of London, and topotypic specimens from Cruz del Eje (*Graomys centralis*), Chumbicha (*G. medius*), and Cachi (*G. cachinus*). The complete list of specimens is provided in the Supporting information (Appendix S2).

The protocol and the general geometric morphometric procedure are similar to that used in a previous study (Martínez & Di Cola, 2011). The images of skulls were taken by J. J. Martínez (JJM). To reduce distortion artefacts, specimens were positioned at the centre of the field of view, and the horizontal position of skulls was checked visually before taking

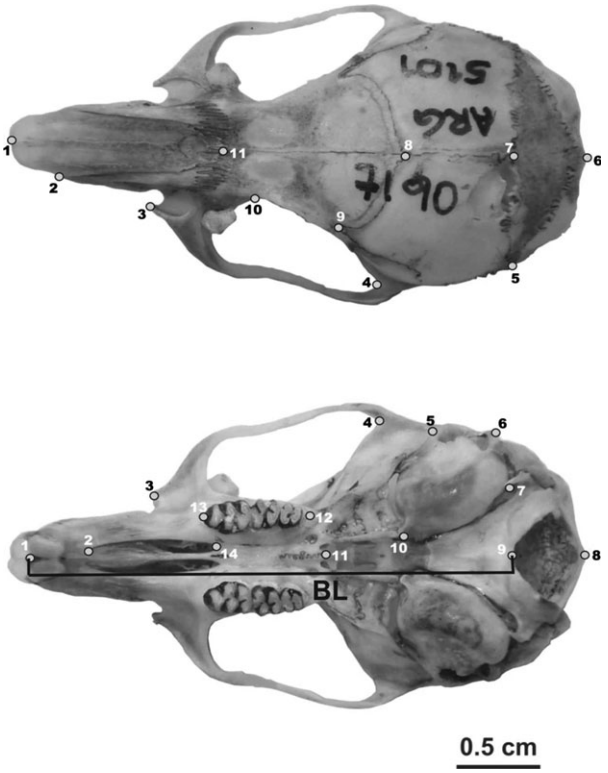

Figure 2. Basal length (BL) of the skull and landmarks captured for this study on dorsal and ventral views. Dorsal view of skull: 1 = rostralmost point of the nasal bone; 2 = intersection of the rostral curvature of the nasal process of the incisive and the nasal bones in a dorsal projection; 3 = rostral end of zygomatic plate; 4 = caudalmost point of orbit; 5 = intersection of the parietal–interparietal and interparietal–occipital sutures; 6 = caudal end of the curvature of the occipital bone; 7 = intersection of the sagittal and parietal-interparietal sutures; 8 = intersection of the coronal and sagittal sutures; 9 = rostralmost point of the parietal bone; 10 = narrowest point of the interorbital region; 11 = intersection of the nasofrontal suture in the midline. Ventral view of skull: 1 = rostralmost point of the upper incisor tooth next to the midline; 2 = rostral end of the rostral palatine fissure; 3 = rostral end of the zygomatic plate; 4 = caudalmost point of the orbit; 5 = rostral end of the external opening of the bony portion of the auditory canal; 6 = caudal end of the external opening of the bony auditory canal; 7 = caudalmost point of the intersection between the tympanic bulla and jugular foramen; 8 = caudal end of the occipital foramen in the midline; 9 = rostral end of the occipital foramen in the midline; 10 = centralmost point of the Eustachian tube; 11 = caudalmost point of the suture between palatine bones and the rostral border of the mesopterygoid fossa; 12 = caudalmost point of the molar row; 13 = rostralmost point of the molar row; 14 = caudal end of the palatine fissure.

Table 2. Sample size for morphometric variation at intra- and interspecific level in *Graomys*

		Skull size		Dorsal shape		Ventral shape	
Species	Ecoregions	*N* pops	*N* BL	*N* pops	*N* shape	*N* pops	*N* shape
Graomys domorum	Yungas	4	7	4	7	4	7
	Dry Chaco	2	3	2	2	2	3
	Total	6	10	6	9	6	10
Graomys chacoensis	Yungas	1	4	1	2	1	2
	Dry Chaco	30	153	31	143	29	135
	Humid Chaco	5	5	5	5	5	5
	Espinal	3	8	3	5	2	3
	Total	39	170	40	155	37	145
Graomys griseoflavus	Yungas	1	1	1	2	1	1
	Dry Chaco	6	17	6	16	6	16
	Espinal	7	20	7	20	7	19
	High Monte	11	34	10	26	11	27
	Low Monte	9	38	9	33	9	34
	Patagonian steppe	3	8	3	8	3	7
	Total	37	118	36	105	37	104

N pops, number of localities included; *N* BL, number of specimens for the basal length of skull; *N* shape, number of specimens for shape variables derived from geometric morphometrics.

photographs. Landmarks were digitized by JJM on one side of the skull to minimize potential influence of any asymmetry. The landmarks were digitized using TPSDIG2 (Rohlf, 2005). The error as a result of the operator (measurement error) was checked by Procrustes analysis of variance on 25% of the specimens *sensu* Yezerinac, Lougheed & Handford (1992). Measurement error was one order of magnitude smaller than total shape variation (14% for dorsal configuration and 9.5% for ventral view).

Skull size was evaluated by means of basal length (BL) of skull (Fig. 2). BL was measured in 298 specimens (Table 2) using a digital calliper to the nearest 0.01 mm. We used BL as a proxy for skull size, aiming to include as many specimens as possible. The incorporation of this variable allowed us the inclusion of more than 20 additional specimens for the analyses of size variation (Table 2). Moreover, we obtained the same patterns of interspecific differentiation when using BL and dorsal and ventral centroid sizes from a previous study (Martínez & Di Cola, 2011). We assessed species differentiation, as well geographical variation, in each species. BL was also used to estimate the allometric component of shape variation.

Interspecific and ecogeographical variation

All landmark configurations were superimposed using the generalized Procrustes analysis in MORPHOJ (Klingenberg, 2011). Aligned Procrustes coordinates and principal component scores were considered as shape variables.

First, significant interspecific and intraspecific shape differences among the three species (*G. chacoensis*, *G. domorum*, and *G. griseoflavus*) were examined using aligned Procrustes coordinates as input in the MORPHOJ linear model option with 10 000 permutations. Intraspecific differences were analyzed according to ecoregions (Fig. 1). Then, we estimated between-group principal component analysis (BG-PCA), using species as the grouping variable, to explore and to visualize shape variation and group differences. BG-PCA preserves the original morphospace produced by the Procrustes fit because it corresponds to a rigid rotation of the Procrustes shape space in the direction of the largest mean group difference (Mitteroecker & Bookstein, 2011; Seetah, Cardini & Miracle, 2012). BG-PCA was performed in PAST, version 3 (Hammer, Harper & Ryan, 2001) using principal component individual scores and mean locality values as input.

We estimated the proportion of size and shape variance among populations relative to total variation in each species (i.e. *G. chacoensis* and *G. griseoflavus*) using the localities with three or more specimens; thus, for *G. chacoensis*, we used 17 populations for BL, 14 populations for dorsal shape, and 13 for the ventral view of the skull. In *G. griseoflavus*, we used 13 populations for the estimations on BL, dorsal, and ventral shape. The estimation of the percentage of variance as a result of a between

populations component was performed with a linear model using localities as the grouping variable. The statistical significance of the percentage of variation because of differentiation among populations was evaluated using 10 000 permutations.

Matrix correlation and direction of variance

The assessment of the phenotypic V/CV (based on measurements of traits) is much easier to infer than G (Renaud & Auffray, 2013). The P matrix as a proxy for G has been used in several studies (Polly, 2005; Renaud, Auffray & Michaux, 2006; Renaud, Pantalacci & Auffray, 2011). Individual Procrustes coordinates were averaged by localities and the among-localities variation was summed up by means of PCA. A series of matrix correlations between V/CV matrices was performed using MORPHOJ to test the similarity between different degrees of variation (intrapopulation variation, total variation, among-localities variation, within *G. chacoensis* variation, and within *G. griseoflavus* variation). A matrix permutation test (Cheverud, Wagner & Dow, 1989) was used to test the association. This test evaluates the matrix correlation against the null hypothesis that there is no relationship between the matrices.

As a result of an appropriate sample size, intrapopulation V/CV was estimated in a population referred to as DOM ($N = 31$ and 29 for dorsal and ventral views, respectively) belonging to *G. chacoensis*. The size–shape relationship was assessed by calculating directions of allometry by multiple regressions between BL and Procrustes coordinates at intrapopulation and species levels in MORPHOJ. The correlation between the main directions of phenotypic variation (i.e. the first eigenvector of the V/CV matrix or P_{max}, the vector of among-population differentiation, and allometric change) was also estimated inferring the angle between the two vectors, which is the arccosine of the inner product of the two vector elements implemented. The angles and their statistical significance against the null hypothesis of the vectors having random directions in the shape tangent space were estimated in MORPHOJ (Klingenberg & Marugán-Lobón, 2013).

Testing hypothesis of genetic drift in skull shape

We used Lande's method to determine whether the skull shape variation can be explained by genetic drift using a regression between the components of the V/CV matrix derived from DOM (within-population V/CV) on the components of the between-population V/CV matrix for each species. The PCs of the within-population V/CV matrix are ordered by their level of eigenvalues and are uncorrelated. The PC scores of the between-population V/CV matrix were calculated by multiplying the Procrustes coordinate means of each population by the standardized within-populations loadings. Subsequently, the between-population variance for each PC was estimated as the variance among these population mean PC scores (Ackermann & Cheverud, 2004). Under neutral evolution, Lande's model predicts that the between-population variance will be proportional to the within-population variance because $B \propto W(t/N_e)$, where B is the between-population V/CV matrix, W is the within-population V/CV and (t/N_e) is a constant for any particular comparison. Thus, a regression analysis was conducted between the within-population variance on the between-population variance. If differentiation was produced by genetic drift, we expect a regression slope of 1.0; a significant deviation from a slope of 1.0 indicated a pattern unlikely to have been produced by genetic drift.

RESULTS

Systematics and date of divergence

Graomys was recovered as monophyletic with high support values (posterior probability of 1.00; 100% of bootstrap and jackknife) (Fig. 3). The sister relationship between *G. chacoensis* and *G. domorum* was also supported (posterior probability of 0.99; 83% of bootstrap and 80% of jackknife).

The phylogenetic results of the mitochondrial dataset (*mt-cyb*, ND3, and control region) are provided in the Supporting information (Fig. S1). High support values confirm that the genus *Graomys* is recovered as monophyletic. Support values for the sister relationship *G. chacoensis* and *G. domorum* improved when the ND3 and control regions were included: posterior probability of 0.95; 81% and 88% of bootstrap and jackknife supports (see Supporting information, Fig. S1). The results from the nuclear dataset (i.e. IRBP and RAG1) were slightly different regarding the resolution of phylogenetic relationships within *Graomys* (see Supporting information, Fig. S2). Only the specimens of *G. chacoensis* were recovered as monophyletic with low Bayesian support, whereas the specimens of *G. griseoflavus* and *G. domorum* clustered into an unsolved polytomy.

By placing the *Auliscomys* fossil date as a calibration point, the estimated divergence dates were earlier than the estimations derived from the crown divergence of Phyllotini (Parada *et al.*, 2013) (not shown). The chronogram depicting the dates of divergence is shown in Figure 3. The phyllotines would have radiated approximately 5.14–7.11 Mya [95% confidence interval (CI)] in the late Miocene. The

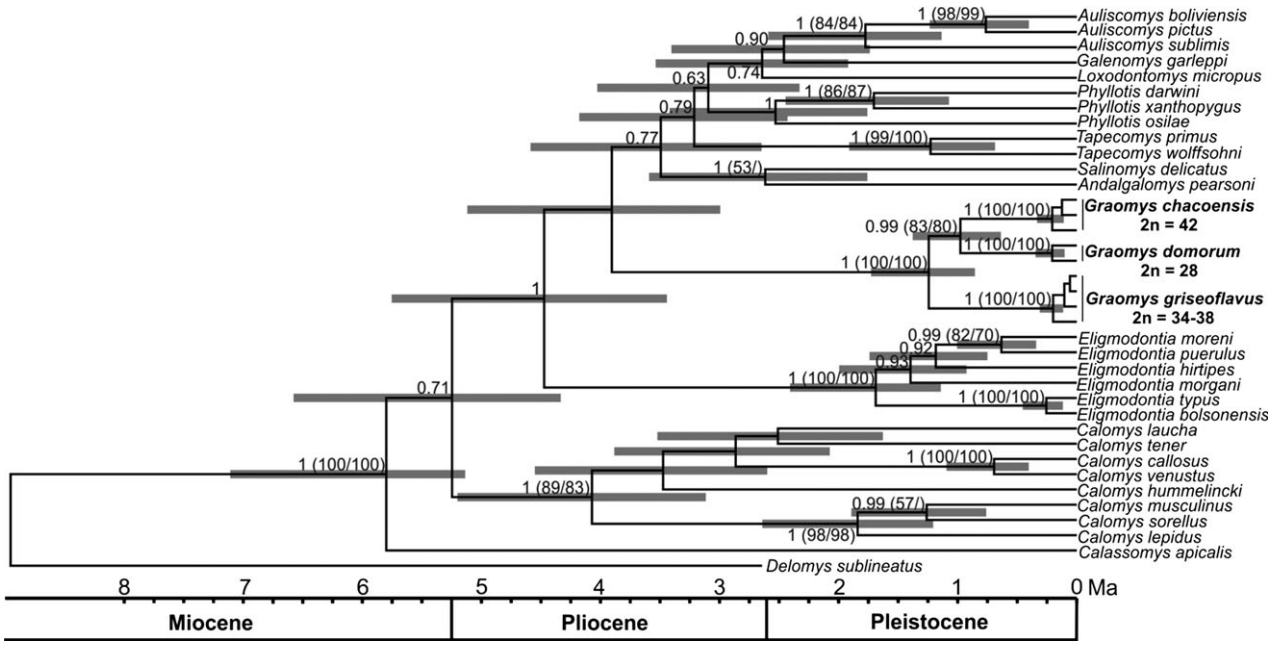

Figure 3. Chronogram depicting the node age estimations by means of molecular clock dating in Phyllotini radiation. The relaxed molecular clock was obtained using a Bayesian inference of the partitioned matrix (*mt-cyb*, ND3, control region, IRBP, and RAG1) gene sequences implemented in BEAST, version 1.8. Bars at the nodes represent the 95% highest posterior density credibility interval of node's age obtained from tree compilation after burn-in period of two independent runs. The values above branches represent posterior probability for Bayesian inference obtained by means of partitioned analysis of five markers (*mt-cyb*, ND3, control region, IRBP, and RAG1); bootstrap and jackknife resampling methods between parentheses, respectively, for parsimony analysis (1 tree, length= 3955, consistency index = 0.455, retention index = 0.571). Only values above 50% are indicated.

common ancestor of *Graomys* and other phyllotines such as *Phyllotis*, *Auliscomys*, *Andalgalomys*, *Salinomys*, *Loxodontomys*, and *Galenomys* could have diverged at 2.99–5.12 Mya (95% CI). The results indicate that *G. griseoflavus* split approximately 0.86–1.73 Mya (95% CI) (median = 1.24 Mya), whereas *G. chacoensis* and *G. domorum* would have diverged approximately 0.64–1.38 Mya (95% CI) (median = 0.98 Mya) in the middle Pleistocene.

Phylogeography and ancestral population location reconstruction

An 1143-bp segment of the *mt-cyb* gene was analyzed in 84 *Graomys* specimens: two *G. domorum*, 26 *G. chacoensis*, and 56 *G. griseoflavus*. Twenty-five segregating sites were identified in *G. chacoensis* and 32 in *G. griseoflavus*. Both haplotype diversity (h) and nucleotide diversity (π) were higher in *G. chacoensis* ($h = 0.948 \pm 0.034$; $\pi = 0.00847$) than in *G. griseoflavus* ($h = 0.899 \pm 0.031$; $\pi = 0.00695$).

When we explored the relationships between clades and the geographical origin of the specimens, we found that there was no clear geographical structure in *G. chacoensis* and *G. griseoflavus*, despite the wide range of habitats in which it occurs (Fig. 4). For example, three specimens from the north of the Gran Chaco ecoregion formed a clade together with one specimen from the southern part of the species distribution; one specimen from locality 5, collected 6 km away from locality 6, clustered in the unresolved major clade composed of specimens from central Argentina.

Intra- and interspecific genetic distances are shown in Table 3. The genetic distance between the two individuals of *G. domorum* was 1.45%, whereas the intraspecific distances were lower in the other two species. The divergence between *G. domorum* and the other two species was higher than between *G. chacoensis* and *G. griseoflavus*, which had very similar values (between 9.6% and 11%).

The genetic differentiation among species resulting from hierarchical AMOVA analysis is shown in Table 4. The main source of variation was among species (90.92%; $P < 0.0001$). AMOVA for each species (the analysis was not performed in *G. domorum* as a result of a low sample size) revealed stronger genetic differentiation in *G. chacoensis* ($\Phi_{ST} = 0.539$; $P < 0.0001$) than in *G. griseoflavus* ($\Phi_{ST} = 0.321$; $P < 0.001$).

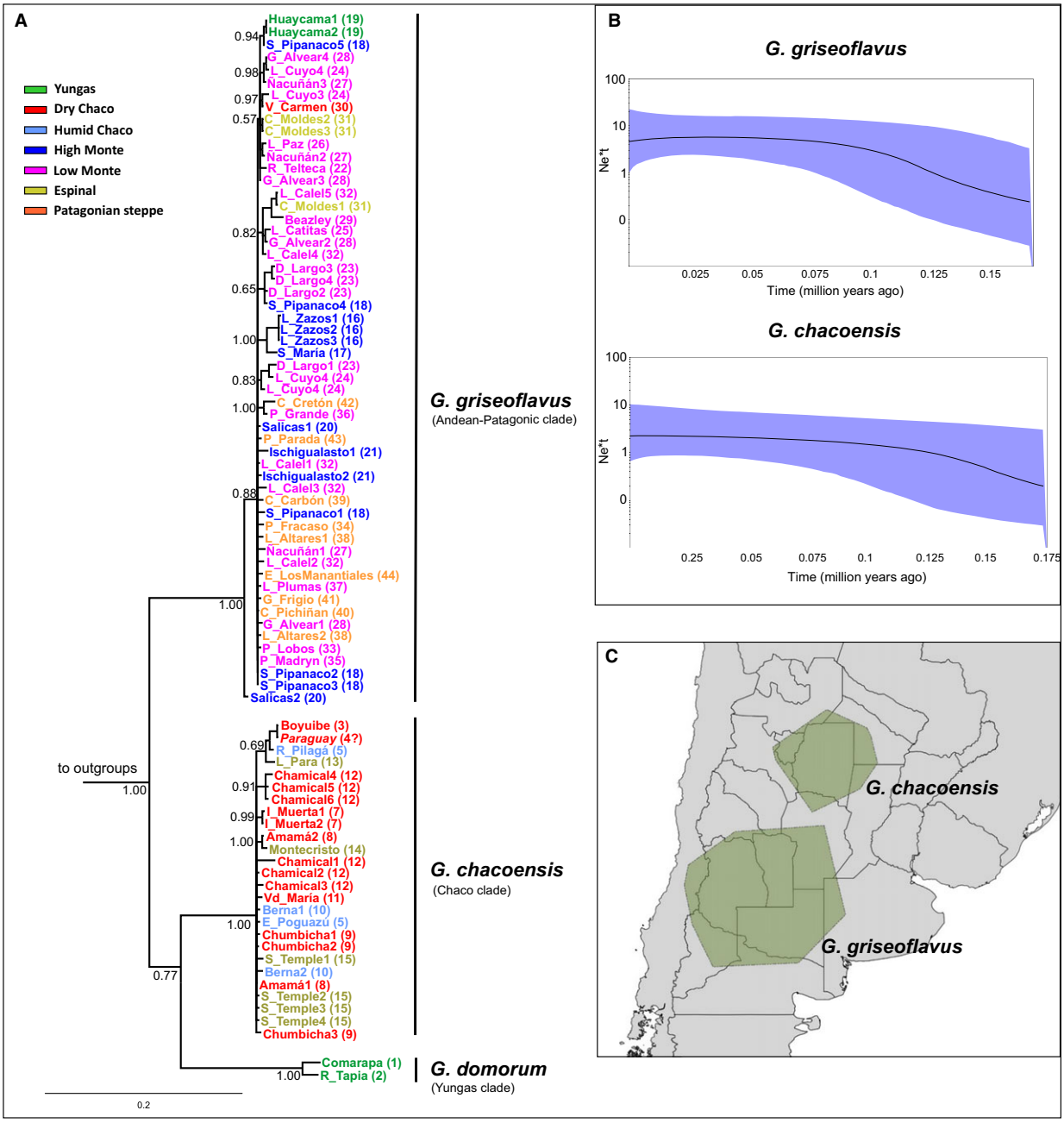

Figure 4. Phylogeographical analysis of *mt-cyb* sequences in *Graomys*. A, phylogram of 50% majority-rule consensus obtained by means of Bayesian inference. Details of the relationships between specimens in three species of *Graomys* according to the ecoregions. The terminals of *Graomys* specimens represent the localities (Fig. 1) and vouchers are described in the Supporting information (Table S1). The values above branches represent posterior probability for Bayesian inference. B, Bayesian skyline plot (BSP) for each species (*Graomys chacoensis* and *Graomys griseoflavus*). Time in million years since present is shown on the *x*-axis. Effective population size multiplied by generational time is shown on the *y*-axis. C, ancestral geographical location analysis implemented in PHYLOMAPPER for *G. chacoensis* and *G. griseoflavus* from 100 replicate runs accounting for phylogenetic uncertainty in *mt-cyb* gene tree.

We found significant deviation from neutrality in both species (Table 5), compatible with demographic changes, population structure or selective pressures. Mismatch distribution analyses were unimodal (not shown) and nonsignificant according to the null hypothesis of demographic and geographical expansions

Table 3. Values of Kimura-two-parameters genetic distances estimated within and between species using *mt-cyb* sequences

	Graomys domorum	*Graomys chacoensis*	*Graomys griseoflavus*
Graomys domorum	**0.0145 (0.0063)**		
Graomys chacoensis	0.1104 (0.0192)	**0.0089 (0.0020)**	
Graomys griseoflavus	0.1007 (0.0179)	0.0961 (0.0163)	**0.0070 (0.0016)**

Values on the diagonal and shown in bold are intraspecific genetic distances. Mean interspecific genetic distances are below the diagonal. Standard error is indicated in brackets.

Table 4. Hierarchical analysis of the molecular variance based on *mt-cyb* sequences in the three species of *Graomys*

Source of variation	Degrees of freedom	Variance	% Total	*P*	Fixation indices
Between species	2	16.546	90.92	< 0.0001	$F_{ct} = 0.909$
Among populations within species	41	0.659	3.62	< 0.0001	$F_{st} = 0.945$
Within populations	40	0.993	5.46	< 0.0001	$F_{sc} = 0.399$
Total	83	18.198			

(Table 5). These results confirm that both species underwent geographical and demographic expansion. The BSPs (Fig. 4) indicate that these demographic changes could have occurred between 150 000 and 175 000 years ago.

The results of 100 PHYLOMAPPER analyses are shown in Figure 4. The ancestral location of *G. griseoflavus* was reconstructed as being in the Monte desert, in central Argentina. For *G. chacoensis*, the ancestral location appears in the Chaco ecoregion, in in northern Argentina.

Interspecific and ecogeographical variation

The interspecific differences in size and shape were highly significant ($P < 0.0001$); however, the percentage of size and shape variance explained by species differences was 9.06%, 3.58%, and 5.19% for BL, dorsal, and ventral shapes, respectively. *Graomys chacoensis* have a smaller skull than the other two species (Fig. 5A), whereas the difference between *G. domorum* and *G. griseoflavus* is subtle. The BG-PCA (Fig. 6A, B) suggests that *G. domorum* is the most distinguishable species, whereas a considerable overlap is evident between the other two species, except for ventral landmark configurations. In this latter case, when the two-first BG-PCs are considered, a group difference between *G. chacoensis* and *G. griseoflavus* is observed. The allometric component was variable between species (Fig. 7C): the percentage of size influence on dorsal shape in *G. chacoensis* was 13.86% ($P < 0.0001$), whereas this reached 20.19% ($P < 0.0001$) for ventral shape. In *G. griseoflavus*, we found significant allometry for dorsal and ventral shape: 24.77% and 19.86% ($P < 0.0001$), respectively.

G. chacoensis presents low morphological differentiations when we consider ecoregions as a proxy for geographical variation. Ecoregions explained 2.4% ($P > 0.05$) of skull size variation (Fig. 5B), and 2.07% ($P > 0.05$) and 4.79% ($P < 0.001$) of dorsal and ventral shape variation (Fig. 7A, B), respectively. Populations belonging to the Humid Chaco, Espinal and Yungas are more different and tend to cluster

Table 5. Results of neutrality tests (Fu's F_S and Tajima's *D*) and demographic and spatial expansions models performed in *Graomys chacoensis* and *Graomys griseoflavus*

	Sudden expansion		Spatial expansion		Neutrality tests	
Species	SSD	Raggedness	SDD	Raggedness	F_S	*D*
Graomys chacoensis	0.017	0.036	0.007	0.036	−14.251***	−1.874*
Graomys griseoflavus	0.002	0.024	0.001	0.024	−25.355***	−1.965**

SSD, sum of squared deviations. *$P < 0.05$, **$P < 0.01$, ***$P < 0.001$.

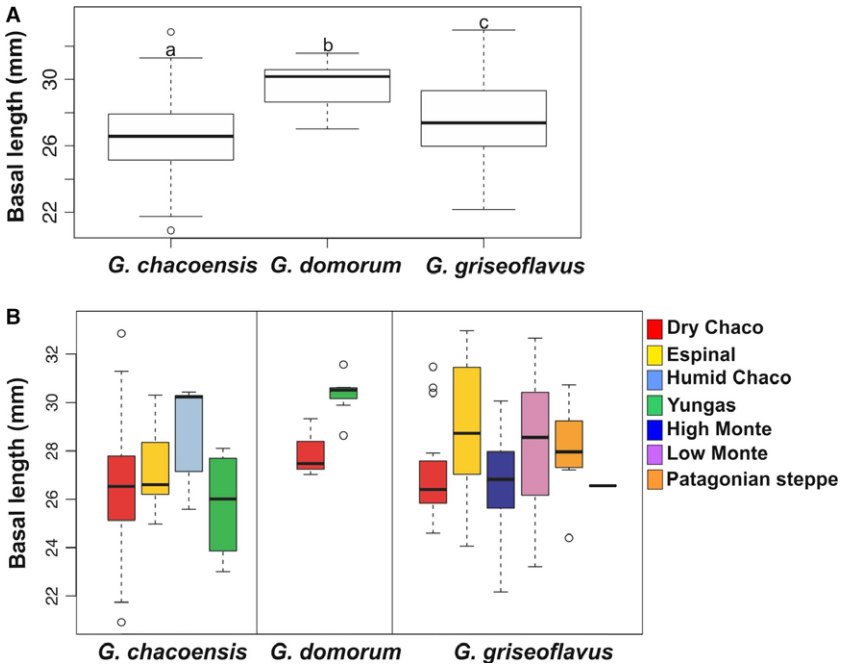

Figure 5. Box-and-whisker plot showing inter- and intraspecific variation of basal length (BL) of the skull in *Graomys*. A, interspecific differences and ranges of variation in BL. B, intraspecific differences and ranges of variation according to the ecoregions in the three species of *Graomys*.

together. On the other hand, *G. griseoflavus* shows marked geographical regionalization of its phenotypic variation: 9.5% ($P < 0.01$), 9.73% ($P < 0.01$), and 12.89% ($P < 0.0001$) of variation in skull size (Fig. 5B), dorsal, and ventral shape variation (Fig. 7A, B), respectively, was accounted by differences in the ecoregions. Specimens from the ecoregions Espinal, Low Monte, and the Patagonian steppe tend to present larger skull than specimens from other ecoregions. For the dorsal shape of skull, populations from the Dry Chaco tend to cluster together, whereas populations from the Low and High Monte tend to differentiate across the first principal component. On the other hand, populations belonging to the Dry Chaco and the Espinal tend to differentiate from the other ecoregions and their localities cluster together in morphospace defined by the ventral shape of skull.

Linear models revealed significant differences ($P < 0.001$) among populations (despite the ecoregions) for each species, as well as for BL and each cranial view. The variance explained by the differences among populations was greater in *G. griseoflavus*, reaching 45.17% for BL, and reaching 31.81% and 38.43% for dorsal and ventral views, respectively. In *G. chacoensis*, the variance accounted by the differences among populations was 17.02% for BL, whereas variance was 20.36% and 26.81% for dorsal and ventral views, respectively.

Direction of shape variance and the role of genetic drift

The V/CV matrix correlation between DOM and the total dorsal variation was high ($r = 0.898$; $P < 0.0001$) and similar to those found between DOM and among-localities in *G. chacoensis* ($r = 0.887$; $P < 0.0001$) and *G. griseoflavus* ($r = 0.791$; $P < 0.0001$). When the P_{max} was analyzed, we found high correlations between the P_{max} vector for DOM and the P_{max} of total variation (angle = 28.53°; $P < 0.0001$), as well as between P_{max} for DOM and the P_{max} of among-localities variation in *G. chacoensis* (angle = 20.58°; $P < 0.0001$). However, this correlation was moderately weak (angle = 37.02°; $P < 0.0001$) when the among-population variation in *G. griseoflavus* was considered. For ventral shape, the results were similar: the V/CV matrix correlation between DOM and the total ventral variation was high ($r = 0.849$; $P < 0.0001$) and similar to those found between DOM and among-localities in *G. chacoensis* ($r = 0.752$; $P < 0.0001$) but moderately high in *G. griseoflavus* ($r = 0.674$; $P < 0.0001$). When the P_{max} was analyzed, we found high correlations between the P_{max} vector for DOM and the P_{max} of total variation (angle = 30.43°; $P < 0.0001$); however the angular correlations were moderately weak between the P_{max} for DOM and the P_{max} of among-localities variation in *G. chacoensis* (angle = 40.65°;

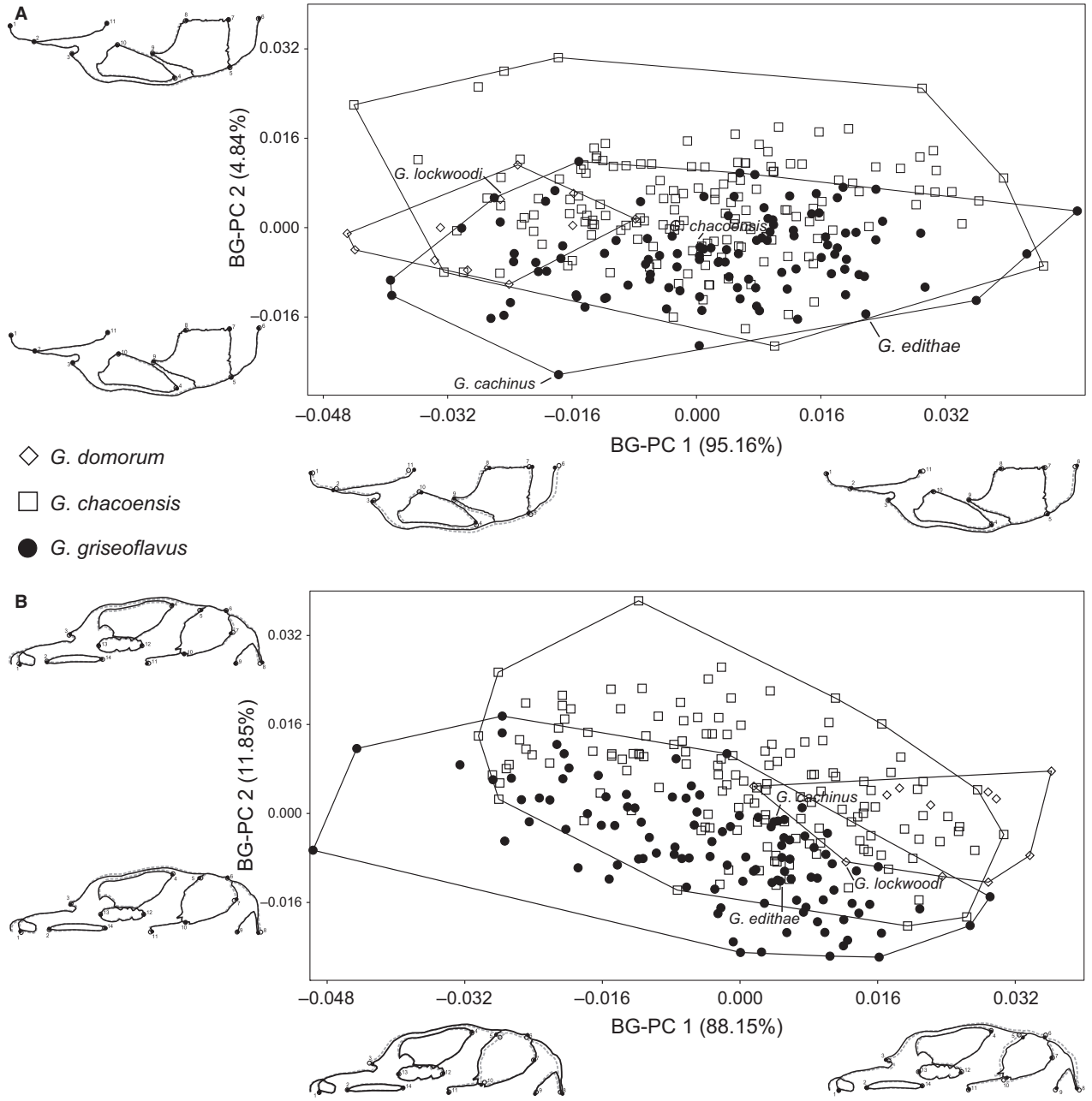

Figure 6. Between-group principal component analysis of interspecific shape variation in *Graomys*. A, dorsal landmark configuration of the skull. B, ventral landmark configuration of the skull. The first two components account for all of the variation between group means. Each symbol represents an individual. Holotypes are indicated by means of arrows. Shape changes (× 2) are indicated for the extreme of each axis, which were obtained considering ordinary principal component analysis of group means. Empty diamonds: *Graomys domorum*; empty squares: *Graomys chacoensis*; black dots: *Graomys griseoflavus*.

$P < 0.0001$) and in *G. griseoflavus* (angle = 52.51°; $P < 0.01$).

Table 6 shows the results of Lande's method when aiming to assess whether skull shape variation in each species can be explained by genetic drift. Both cranial views suggest that genetic drift is a probable evolutionary force for the skull shape in *G. chacoensis*, whereas, in *G. griseoflavus*, both cranial views allow rejection of the null hypothesis for genetic drift because the regression slope differs from 1.00. The results for the ventral view of *G. domorum* suggest a scenario other than genetic drift, whereas dorsal

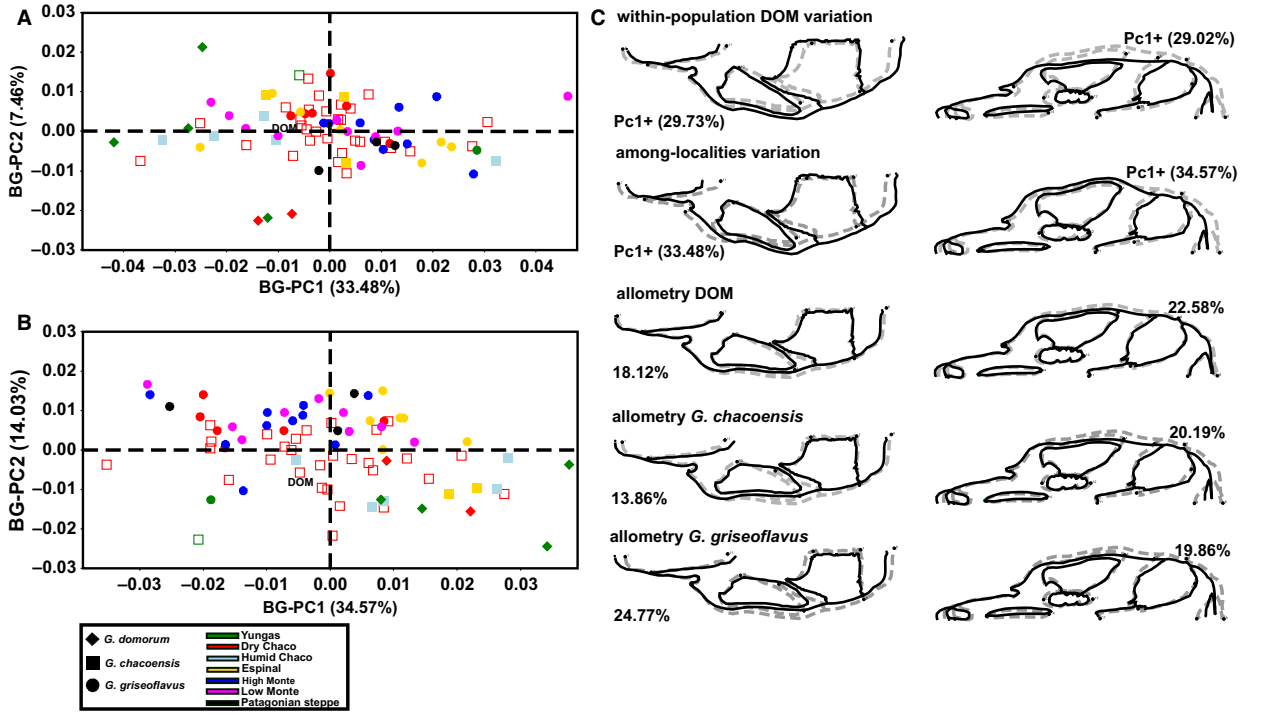

Figure 7. Morphological differentiation of the skull among localities of *Graomys* according to the ecoregions, morphospace was estimated by means of between-group principal component analysis using species as the grouping variable. Each symbol represents a locality. A, morphospace of the dorsal skull shape. B, morphospace of the ventral skull shape. C, shape changes associated at different levels of variation (i.e. intrapopulation, among-localities, and allometry).

shape implies nonconclusive results regarding the main evolutionary driver.

DISCUSSION

Species limits and phylogenetic relationships in *Graomys*

The molecular phylogenetic analyses carried out on *mt-cyb*, mitochondrial, and total datasets revealed three main clades belonging to *G. griseoflavus*, *G. chacoensis*, and *G. domorum*. The analyses on nuclear markers failed to recover the three clades belonging to the species under study. It is well documented that, in mammals, nuclear genes can have 11–62-fold lower rates of substitution than mtDNA genes (Lynch, Koskella & Schaack, 2006); the species of *Graomys* are relatively new and nuclear genes might not yet have reached reciprocal monophyly.

The monophyly of *Graomys* has previously been supported using molecular characters. However, the relationships within the genus were only scarcely assessed. Our results confirm the monophyletic nature of *Graomys* as inferred from the mitochondrial and nuclear data. The clade comprising *G. chacoensis* and *G. domorum* showed low statistical support when using only *mt-cyb* sequences, despite an interspecific distance between species pairs of appproximately 10%. However, when we included two additional mitochondrial markers (ND and control

Table 6. Results of regression analysis of among- population on within-population variance as a test for genetic drift

Skull view	Species	Consistent with drift?	Slope *b*	95% confidence interval	r^2	*P*
Dorsal	*Graomys chacoensis*	Yes	0.690	0.624 1.02	0.886	< 0.0001
	Graomys griseoflavus	No	0.613	0.528 0.859	0.881	< 0.0001
	Graomys domorum	Nonconclusive	0.839	0.099 1.065	0.725	< 0.0001
Ventral	*Graomys chacoensis*	Yes	0.741	0.662 1.022	0.879	< 0.0001
	Graomys griseoflavus	No	0.692	0.371 0.860	0.837	< 0.0001
	Graomys domorum	No	0.579	−0.025 0.755	0.527	< 0.0001

region) in a joint phylogenetic analysis, we obtained high support for this relationship. The sisterhood between these two species was also confirmed when the partitioned analysis of five markers including nuclear DNA was carried out.

Previous morphological and cytogenetic evidence contradicts the molecular phylogenetic results. According to Theiler & Gardenal (1994), *G. griseoflavus* and *G. chacoensis* cannot be distinguished by analyses of external and morphological characters; *G. domorum* is the most distinguishable species, suggesting that *G. griseoflavus* and *G. chacoensis* are sister species. Regarding cytogenetic studies, Pearson & Patton (1976), Zambelli *et al.* (1994), Theiler & Blanco (1996b), Catanesi *et al.* (2002), and Lanzone *et al.* (2014) reported high chromosomal polymorphism in *G. griseoflavus*, with a diploid number ranging from 33 to 38. *Graomys chacoensis* presents $2n = 42$ and *G. domorum* has $2n = 28$. Based on cytogenetic evidence, *G. chacoensis* was defined as the ancestral species that gave origin to the other species as a result of subsequent Robertsonian fusions. This evolutionary model is outdated and is not in line with the results of molecular phylogenetics in the present study.

A specimen of *G. domorum* from north-westhern Argentina is included for first time in a molecular phylogenetic analysis. It appears to be related more to the *G. domorum* specimen from Bolivia than to any other specimen of *G. griseoflavus* and *G. chacoensis* from Argentina. However, the value of 1.45% for the genetic distance between these two individuals highlights the need to capture more specimens from the entire geographical range of this species to enable a more reliable taxonomic inference. Besides, a comparison with specimens from Bolivia should be performed to provide evidence on cranial affinities with Argentine specimens assigned to *G. domorum*.

The inclusion in our morphometric analyses of type material of *Graomys* with debatable taxonomic status, such as as *G. edithae* or *G. lockwoodi*, provided significant information about phenotypic similarity among the valid species of the genus, especially those with a wide ecogrographical distribution. The skull shape of *G. edithae* is morphologically similar to that of *G. griseoflavus* (see Supporting information, Figures S3, S4). According to Thomas (1919), the skull morphology of *G. edithae* is a miniature version of that of all the other species of the genus, having suprorbital edges without beading. Our results suggest that the specimen of *G. lockwoodi* is similar to those of *G. domorum* (see Supporting information, Figure S3 and S4). Thomas (1918) noted out that the tympanic bullae of *G. lockwoodi* are larger than in *G. domorum* and smaller than in *G. cachinus*. We confirmed this statement partially; the specimen of *G. lockwoodi* presents a different tympanic bullae shape and, overall, it is wider than the mean shape of the specimens of *G. domorum*.

Graomys cachinus tend to be the most distinguishable species with respect to the mean shapes of the valid species. This species was described in a valley region at the foot of the Nevados del Cachi > 2500 m a.s.l. Particular environmental conditions likely modelled the skull shape of *G. cachinus*. Allen (1901) argued that *G. cachinus* differs from *G. griseoflavus* with respect to its wider skull, from the rostrum to the braincase. He concluded that this species has an upper molar tooth row one-third wider and longer than that of *G. griseoflavus*, and that *G. chacoensis* differs from *G. cachinus* with respect to smaller tympanic bullae and greater interparietal distance. The results of our geometric morphometric procedures could not determine the phenotypic affinities of the nominal form *G. cachinus* as a result of incongruence between morphospaces: when dorsal shape is considered, *G. cachinus* is more similar to *G. griseoflavus* than to the other species; in contrast, the ventral shape indicates that *G. cachinus* is similar to *G. chacoensis*. We emphasize that the differences reported in the original descriptions have weak support when we include a wide sampling of specimens in the geometric approach. The mean shape of *G. griseoflavus* displays a slightly wider braincase than *G. cachinus*, although their tooth molar rows are very similar in length. *Graomys cachinus* has longer nasals than *G. griseoflavus* and *G. chacoensis*, being longer in the former; *G. cachinus* also has a narrower interorbital region than the average shapes of the other two. The holotype of *G. chacoensis* falls within the overlap area between *G. griseoflavus* and *G. chacoensis*. Given the conservative nature of skull morphology in the genus, the validation of *G. edithae*, *G. lockwoodi*, and *G. cachinus* requires additional evidence obtained via morphology, molecular markers, and cytogenetics in specimens collected from each type locality.

Phylogeographical and ecogeographical patterns

The analysis of intraspecific patterns showed a non-defined phylogeographical structure in *G. chacoensis* and in *G. griseoflavus*. The results reported in the present study suggest recent demographic and geographical expansions in both species approximately 150 000–175 000 years ago. Our results are in agreement with those of Lessa, D'Elía & Pardiñas (2010) for Patagonian localities of *G. griseoflavus*, with a mean value of 100 000 years ago. The last glacial period occurred during the last 100 000 years of the Pleistocene; in this period of cold–dry climates, there

was a contraction of the areas occupied by subtropical and tropical biomes, resulting in the concomitant expansion and interconnection of open biomes (Ortiz-Jaureguizar & Cladera, 2006). Expansion of open biomes likely triggered the geographical and demographic expansion of *G. chacoensis* and *G. griseoflavus*.

The presence of an apparent phylogeographical 'break' in the northern part of the distribution in *G. chacoensis*, which includes specimens from the Bolivian, Paraguayan, and Argentinean Chaco ecoregion, is worthy of note. Based on patterns of bird diversity and distribution, Nores (1992) proposed the occurrence of a corridor of approximately 200 km wide in the Quaternary, connecting the two areas of tropical forest in the Southern Cone: the Yungas and the Atlantic forest. This connection may have interrupted the Chaco continuity, generating the northern and the southern Chaco. This vicariant process may have resulted in the observed phylogeographical break in *G. chacoensis*. The recovery of different haplotype clades for specimens captured in localities separated by < 6 km suggests the occurrence of secondary contact in the area. A comparative phylogeographical study of different rodent species inhabiting the Chaco might clarify this aspect.

Taking into account the percentage of variance explained, the phenotypes tend to diverge more locally than geographically across the ecoregions (17–45% and 2–13%, respectively) (Fig. 7), suggesting that differences in the local habitat (environmental and ecological conditions) have a greater effect on the phenotypes than regional conditions and floral compositions; some of this local variance is probably of plastic origin because the skull can remodel through time in response to the functional demand. Indeed, niche modelling predicted a high ecological interchangeability with a broad region of distributional overlap between *G. griseoflavus* and *G. chacoensis* (Martínez & Di Cola, 2011), although this must be limited by additional factors other than the climatic factors not considered in the models; the real distributional overlap could be restricted to transition zones between the two main ecoregions (i.e. the Monte desert and the Chaco).

The skull size variation in *G. griseoflavus* presents a geographical pattern in which specimens from the southern ecoregions, such as as Espinal, Low Monte, and the Patagonian steppe, tend to have skulls larger than those of individuals from other ecoregions. This is coincident with the positive correlation of skull size with temperature seasonality and the minimum temperature of the coldest month (Martínez & Di Cola, 2011), which are higher in southern South America. Especially in the driest climates, larger bodies could be an adaptation to water conservation (James, 1970).

Modes of diversification

Graomys undoubtedly comprises an excellent small mammal model for studying the mechanisms and modes of speciation, as are *Mus musculus* (Jones & Searle, 2015), the genus *Spalax* (Hadid *et al.*, 2013), and the Neotropical *Ctenomys* (Caraballo, Abruzzese & Rossi, 2012). Independently of the mechanism that promoted speciation in *Graomys*, the mode of speciation (i.e. the geographical context) is an interesting topic of analysis. The geographical location for the ancestor of *G. griseoflavus* could be placed in central-western Argentina. In *G. chacoensis*, the Chaco ecoregion in north-western Argentina was recovered as the ancestral area, which presents floristic affinities with the Yungas Montane forest (Cabrera & Willink, 1980) near to the current distribution of *G. domorum*. The results of the present study are consistent with the proposal of Braun (1993) suggesting that the genus would have originated in a transitional region between the Chaco and the Monte in Central Argentina, and subsequently might have dispersed to the Pampean ecoregion, which is coincident with the presence of the extinct *G. dorae* in the upper Pliocene (Reig, 1978). The use of a relaxed molecular clock in a phylogenetic context reveals a recent process of speciation probably promoted by both chromosomal rearrangements and environmental change: *G. griseoflavus* could have split approximately 0.86–1.73 Mya, whereas the estimation for the split between *G. chacoensis* and *G. domorum* was 0.64–1.38 Mya.

Skull morphology among species of *Graomys* has lower levels of differentiation than karyotype and genetic variation, with *G. chacoensis* and *G. griseoflavus* being more similar in this respect; however, molecular phylogenetics suggests a close relationship between *G. chacoensis* and *G. domorum*. This last species is the most distinguishable in external and skull morphologies and in diploid numbers ($2n = 28$ versus $2n = 33$–38 of *G. griseoflavus* and $2n = 42$ of *G. chacoensis*).

We were unable to hypothesize about cranial evolution in *G. domorum* for the dorsal shape, whereas ventral shape may indicate that this character evolved under selection. The populations of *G. chacoensis* could have diverged under genetic drift, probably reflecting the lack of morphometric differentiation among ecoregions, whereas, in the populations of *G. griseoflavus*, our evidence indicates that both characters reject the hypothesis of evolution under genetic drift. *G. griseoflavus* presents a wider geographical distribution encompassing more ecoregions than the

other two species; therefore, a major morphometric differentiation among populations/ecoregions in this species could be expected.

The P matrix can fluctuate over short periods or stabilize over longer ones. Renaud *et al.* (2006) showed that the P matrix and P_{max} of tooth shape were conserved in two lineages of murine rodents spanning over 10 Myr of evolution, whereas Polly (2005) suggested a rapid evolution of the molar shape P matrix in modern insular populations of *Sorex araneus*. Our results indicate that the patterns of intraspecific phenotypic variation are conserved over long evolutionary timescales for the skull shape in *Graomys* (i.e. at least 2 Myr of evolution). Similarly, *G. griseoflavus* and *G. chacoensis* have similarities in V/CV matrices, as well as in P_{max} vectors of phenotypic traits, which, under adequate selection pressures, could generate similar phenotypes. Interestingly, the correlations between P_{max} at the intrapopulation level and among-localities variation in the two species were lower in the ventral than in the dorsal skull shape. This discrepancy could be attributable to the local differentiation of ventral skull shape (which involves mainly changes in the tympanic bullae) and its correlation with environmental variables (Martínez & Di Cola, 2011).

In our attempt to integrate different kinds of characters at the interspecific level, the present study highlights the complex diversification process of *Graomys* that involves decoupling of the evolution of morphological, karyological, and molecular traits, probably as a result of different response to selection and genetic drift in local populations.

ACKNOWLEDGEMENTS

We are very grateful to the individuals who contributed sample tissues for molecular analysis: Ignacio Ferro, Somky, Cecilia Lanzone, Agustina Ojeda, Rubén Barquez, Ricardo Ojeda, Pablo Teta, Raúl González Ittig, Gerardo Theiler, Stella Giannoni, María Inés Carma, Silvina Bisceglia, Javier Pereira, José Priotto, Valeria Rodríguez, and Adrián Díaz. We also thank those who allowed us to study the specimens under their care: Rubén Barquez (CML) and members of PIDBA; David Flores (MACN); Jaime Polop and José Priotto (CUNRC); and Gerardo Theiler (UNC). We thank Louise Tomsett, Paula Jenkins, and Sally Jennings (BMNH) for the photographs of type specimens of *Graomys*. Ignacio Ferro, Marcos Mollerach, Joaquín Brunet, Lucia Sommaro, Luz Carrizo, Mariano Sánchez, Gerardo Theiler, Raúl González Ittig, Julián Lescano, Cecilia Castilla, and Sabrina Villalba assisted us in the field. We are especially grateful to Ignacio Ferro for all of his help and support during different parts of the present study. We are grateful to Rodrigo Lima, Rodrigo Fornel, and two anonymous reviewers for their corrections, which significantly improved the manuscript. JJM and CNG are career researchers of CONICET. This contribution is part of the doctoral thesis of JJM carried out at the Universidad Nacional de Córdoba (UNC). The Secretaría de Ciencia y Técnica (UNC) partially funded this work.

REFERENCES

Ackermann RR, Cheverud JM. 2004. Detecting genetic drift versus selection in human evolution. *Proceedings of the National Academy of Science of the United States of America* **101:** 17946–17951.

Allen JA. 1901. New South American Muridae and a new *Metachirus*. *Bulletin of the American Museum of Natural History* **14:** 405–412.

Anderson S. 1997. Mammals of Bolivia, taxonomy and distribution. *Bulletin of the American Museum of Natural History* **231:** 1–652.

Anderson S, Yates TL. 2000. A new genus and species of phyllotine rodent from Bolivia. *Journal of Mammalogy* **81:** 18–36.

Braun JK. 1993. *Systematic relationships of the tribe Phyllotini (Muridae: Sigmodontinae) of South America*. Oklahoma Museum of Natural History: Special Publication, 1–50.

Bruford ME, Hanotte O, Brookfield JFY, Burke T. 1992. Single-locus and multilocus DNA fingerprinting. In: Hoelzel AR, ed. *Molecular genetic analysis of populations, a practical approach*. Oxford: Oxford University Press, 225–269.

Cabrera AL, Willink A. 1980. *Biogeografía de América Latina*. Programa Regional de Desarrollo Científico y Tecnológico. Organización de Estados Américanos. Serie Biología 13. Washington, DC.

Caraballo DA, Abruzzese GA, Rossi MS. 2012. Diversity of tucos-tucos (*Ctenomys*, Rodentia) in the Northeastern wetlands from Argentina: mitochondrial phylogeny and chromosomal evolution. *Genetica* **140:** 125–136.

Catanesi CI, Vidal-Rioja L, Crisci JV, Zambelli A. 2002. Phylogenetic relationships among Robertsonian karyomorphs of *Graomys griseoflavus* (Rodentia, Muridae) by mitochondrial cytochrome b DNA sequencing. *Hereditas* **136:** 130–136.

Cheverud JM, Wagner GP, Dow MM. 1989. Methods for the comparative analysis of variation patterns. *Systematic Zoology* **38:** 201–213.

Darriba D, Taboada GL, Doallo R, Posada D. 2012. jModelTest 2: more models, new heuristics and parallel computing. *Nature Methods* **9:** 772.

Díaz MM, Teta P, Pardiñas UFJ, Barquez RM. 2006. Tribu Phyllotini Vorontsov, 1959. In: Barquez RM, Díaz MM, Ojeda RA, eds. *Mamíferos de Argentina. Sistemática y distribución*. Tucumán, Sarem, 175–189.

Drummond AJ, Rambaut A. 2007. Beast: Bayesian evolutionary analysis by sampling trees. *BMC Evolutionary Biology* **7:** e214.

Drummond AJ, Rambaut A, Shapiro B, Pybus OG. 2005. Bayesian coalescent inference of past population dynamics from molecular sequences. *Molecular Biology and Evolution* **22:** 1185–1192.

Drummond AJ, Ho S, Phillips M, Rambaut A. 2006. Relaxed phylogenetics and dating with confidence. *PLoS Biology* **4:** e88.

Drummond AJ, Suchard MA, Xie D, Rambaut A. 2012. Bayesian phylogenetics with BEAUti and the BEAST 1.7. *Molecular Biology and Evolution* **29:** 1969–1973.

Edgard RC. 2004. Muscle: multiple sequence alignment with high accuracy and high throughput. *Nucleic Acids Research* **32:** 1792–1797.

Excoffier L, Lischer HEL. 2010. Arlequin suite ver 3.5: a new series of programs to perform population genetics analyses under Linux and Windows. *Molecular Ecology Resources* **10:** 564–567.

Excoffier L, Smouse PE, Quattro JM. 1992. Analysis of molecular variance inferred from metric distances among DNA haplotypes: application to human mitochondrial DNA restriction data. *Genetics* **131:** 479–491.

Farris JS, Albert VA, Kallersjo M, Lipscomb D, Kluge AG. 1996. Parsimony jackknifing outperforms neighbour-joining. *Cladistics* **12:** 99–124.

Felsenstein J. 1985. Confidence limits on phylogenies: an approach using bootstrap. *Evolution* **39:** 783–791.

Ferro LI, Martínez JJ. 2009. Molecular and morphometric evidences validate a Chacoan species of the grey leaf-eared mice genus *Graomys* (Rodentia: Cricetidae: Sigmodontinae). *Mammalia* **73:** 265–271.

Fu Y-X. 1997. Statistical test of neutrality of mutations against population growth, hitchhiking and background selection. *Genetics* **147:** 915–925.

Goloboff PA. 1999. Analyzing large data sets in reasonable times: solutions for composite optima. *Cladistics* **15:** 415–428.

Goloboff P, Farris J, Nixon K. 2008. TNT, a free program for phylogenetic analysis. *Cladistics* **24:** 774–786.

Granjon L, Montgelard C. 2012. *The input of DNA sequences to animal systematic: rodents as study cases*. DNA sequencing. Methods and applications. Rijeka, Croatia: InTech Publisher. 104–140.

Hadid Y, Tzur S, Pavlíček T, Šumbera R, Šklíba J, Lövy M, Fragman-Sapir Bailes A, Arieli R, Raz S, Nevo E. 2013. Possible incipient sympatric speciation in blind mole rats (*Spalax*). *Proceedings of the National Academy of Sciences of the United States of America* **12:** 2587–2592.

Hammer Ø, Harper DA, Ryan PD. 2001. PAST: paleontological statistics software package for education and data analysis. *Palaeontologia Electronica* **4:** e1.

James FC. 1970. Geographic size variation in birds and its relationship to climate. *Ecology* **51:** 365–390.

Jones EP, Searle JB. 2015. Differing Y chromosome versus mitochondrial DNA ancestry, phylogeography, and introgression in the house mouse. *Biological Journal of the Linnean Society* **115:** 348–361.

Kennedy P, Nachman MW. 1998. Deleterious mutations at the mitochondrial ND3 gene in South American marsh rats (*Holochilus*). *Genetics* **150:** 359–368.

Klingenberg CP. 2011. MorphoJ: an integrated software package for geometric morphometrics. *Molecular Ecology Resources* **11:** 353–357.

Klingenberg CP, Marugán-Lobón J. 2013. Evolutionary covariation in geometric morphometric data: analyzing integration, modularity, and allometry in a phylogenetic context. *Systematic Biology* **62:** 591–610.

Kumar S, Nei M, Dudley J, Tamura K. 2008. MEGA: a biologist-centric software for molecular evolutionary analysis of DNA and protein sequences. *Briefings in Bioinformatics* **9:** 299–306.

Lanzone C, Suárez SN, Rodriguez D, Ojeda A, Albanese S, Ojeda RA. 2014. Chromosomal variability and morphological notes in *Graomys griseoflavus* (Rodentia, Cricetidae, Sigmodontinae), from Catamarca and Mendoza provinces, Argentina. *Mastozoologia Neotropical* **21:** 47–58.

Lemmon AR, Lemmon EM. 2008. A likelihood framework for estimating phylogeographic history on a continuous landscape. *Systematic Biology* **57:** 544–561.

Lessa E, D'Elía G, Pardiñas UFJ. 2010. Genetic footprints of late Quaternary climate change in the diversity of Patagonia-Fueguian rodents. *Molecular Ecology* **19:** 3031–3037.

Lynch M, Koskella B, Schaack S. 2006. Mutation pressure and the evolution of organelle genomic architecture. *Science* **311:** 1727–1730.

Martínez JJ, Di Cola V. 2011. Geographic distribution and phenetic skull variation in two close species of *Graomys* (Rodentia, Cricetidae, Sigmodontinae). *Zoologischer Anzeiger* **250:** 175–194.

Martínez JJ, González-Ittig RE, Theiler GR, Ojeda R, Lanzone C, Ojeda A, Gardenal CN. 2010. Patterns of speciation in two sibling species of *Graomys* (Rodentia, Cricetidae) based on mtDNA sequences. *Journal of Zoological Systematic and Evolutionary Research* **48:** 159–166.

Martínez JJ, Ferro LI, Mollerach MI, Barquez RM. 2012. The phylogenetic relationships of the Andean swamp rat genus *Neotomys* (Rodentia, Cricetidae, Sigmodontinae) based on mitochondrial and nuclear markers. *Acta Theriologica* **57:** 277–287.

McGuigan K, Chenoweth SF, Blows MW. 2005. Phenotypic divergence along lines of genetic variance. *American Naturalist* **165:** 32–43.

Mitteroecker P, Bookstein F. 2011. Linear discrimination, ordination, and the visualization of selection gradients in modern morphometrics. *Evolutionary Biology* **38:** 100–114.

Nores M. 1992. Bird speciation in subtropical South America in relation to forest expansion and retraction. *The Auk* **109:** 346–357.

Olds N, Anderson S. 1989. A diagnosis of the tribe Phyllotini (Rodentia, Muridae). In: Redford KH, Eisenberg JF, eds. *Advances in Neotropical mammalogy*. Gainesville, FL: Sandhill Crane Press, 55–74.

Ortiz-Jaureguizar E, Cladera GA. 2006. Paleoenvironmental evolution of southern South America during the Cenozoic. *Journal of Arid Environments* **66:** 498–532.

Parada A, Pardiñas UFJ, Salazar-Bravo J, D'Elía G, Palma RE. 2013. Dating an impressive Neotropical radiation: molecular time estimates for the Sigmodontinae (Rodentia) provide insights into its historical biogeography. *Molecular Phylogenetics and Evolution* **66:** 960–968.

Pardiñas UFJ, Tonni E. 1998. Procedencia estratigráfica y edad de los más antiguos muroideos (Mammalia, Rodentia) de América del Sur. *Ameghiniana* **35:** 473–475.

Pearson OP. 1972. New information on ranges and relationships within the rodent genus *Phyllotis* in Peru and Ecuador. *Journal of Mammalogy* **53:** 677–686.

Pearson OP, Patton JL. 1976. Relationships among South American phyllotine rodents based on chromosome analysis. *Journal of Mammalogy* **57:** 339–350.

Polly D. 2005. Development and phenotypic correlations: the evolution of tooth shape in *Sorex araneus*. *Evolution and Development* **7:** 29–41.

Rambaut A, Drummond AJ. 2003. Tracer. Available at: http://beast.bio.ed.ac.uk/tracer

Reig OA. 1978. Roedores cricétidos del Plioceno superior de la provincia de Buenos Aires (Argentina). *Publicaciones de Museo Municipal de Ciencias Naturales de Mar del Plata 'Lorenzo Scaglia'* **2:** 164–190.

Renaud S, Auffray J-C. 2013. The direction of main phenotypic variance as a channel to morphological evolution: case studies in murine rodents. *Hystrix* **24:** 85–93.

Renaud S, Auffray J-C, Michaux J. 2006. Conserved phenotypic variation patterns, evolution along lines of least resistance, and departure due to selection in fossil rodents. *Evolution* **60:** 1701–1717.

Renaud S, Pantalacci S, Auffray J-C. 2011. Differential evolvability along lines of least resistance of upper and lower molars in island house mice. *PLoS ONE* **6:** e18951.

Rogers AR, Harpending H. 1992. Population growth makes waves in the distribution of pairwise genetic differences. *Molecular Biology and Evolution* **9:** 552–569.

Rohlf FJ. 2005. *tpsDig2*. Stony Brook, NY: Department of Ecology and Evolution, State University of New York at Stony Brook.

Ronquist F, Huelsenbeck JP. 2003. MrBayes 3: Bayesian phylogenetic inference under mixed models. *Bioinformatics* **19:** 1572–1574.

Salazar-Bravo J, Pardiñas UFJ, D'Elía G. 2013. A phylogenetic appraisal of Sigmodontinae (Rodentia, Cricetidae) with emphasis on phyllotine genera: systematic and biogeography. *Zoologica Scripta* **42:** 250–261.

Schluter D. 1996. Adaptive radiation along lines of least resistance. *Evolution* **50:** 1766–1774.

Seetah TK, Cardini A, Miracle PT. 2012. Can *morphospace* shed light on cave bear spatial-temporal variation? Population dynamics of *Ursus spelaeus* from Romualdova pećina and Vindija, (Craotia). *Journal of Archaeological Science* **39:** 500–510.

da Silva MN, Patton JL. 1993. Amazonian phylogeography: mtDNA sequence variation in arboreal echimyid rodents (Caviomorpha). *Molecular Phyloegenetics and Evolution* **2:** 243–255.

Smith MF, Patton JL. 1999. Phylogenetic relationships and the radiation of sigmodontine rodents in South America: evidence from cytochrome *b*. *Journal of Mammalian Evolution* **6:** 89–128.

Steppan SJ, Phillips PC, Houle D. 2002. Comparative quantitative genetics: evolution of the G matrix. *Trends in Ecology and Evolution* **17:** 320–327.

Steppan SJ, Ramirez O, Banbury J, Huchon D, Pacheco V, Walker LI, Spotorno AE. 2007. A molecular reappraisal of the systematics of the leaf-eared mice *Phyllotis* and their relatives. In: Kelt DA, Lessa E, Salazar-Bravo JA, Patton JL, eds. *The quintessential naturalist: honoring the life and legacy of Oliver P. Pearson*. Oakland, CA: University of California Publications in Zoology, 799–826.

Tajima F. 1989. The effect of change in population size on DNA polymorphism. *Genetics* **123:** 597–601.

Theiler GR, Blanco A. 1996a. Patterns of evolution in *Graomys griseoflavus* (Rodentia, Muridae): III. Olfatory discrimintaion as a premating isolation mechanism between cytotypes. *Journal of Experimental Zoology* **274:** 346–350.

Theiler GR, Blanco A. 1996b. Patterns of evolution in *Graomys griseoflavus* (Rodentia, Muridae): II. Reproductive isolation between cytotypes. *Journal of Mammalogy* **77:** 776–784.

Theiler GR, Gardenal CN. 1994. Patterns of evolution in *Graomys griseoflavus* (Rodentia, Cricetidae). I. Protein polymorphism in populations with different chromosome number. *Hereditas* **120:** 225–229.

Theiler GR, Gardenal CN, Blanco A. 1999. Patterns of evolution in *Graomys griseoflavus* (Rodentia, Muridae). IV. A case of rapid speciation. *Journal of Evolutionary Biology* **12:** 970–979.

Thomas O. 1918. On small mammals from Salta and Jujuy collected by Mr. E. Budin. *Annals and Magazine of Natural History* **9:** 489–500.

Thomas O. 1919. On small mammals from "Otro Cerro", North eastern La Rioja, collected by Mr. E. Budin. *Annals and Magazine of Natural History* **9:** 489–500.

Wainberg RL, Fronza TG. 1974. Autosomic polymorphism in *Phyllotis griseoflavus griseoflavus* Waterhouse, 1837 (Rodentia, Cricetidae). *Bolletino de Zoologia* **41:** 19–24.

Yezerinac SM, Lougheed SC, Handford P. 1992. Measurement error and morphometric studies: statistical power and observer experience. *Systematic Biology* **41:** 471–482.

Zambelli A, Vidal-Rioja L, Wainberg R. 1994. Cytogenetic analysis of autosomal polymorphism in *Graomys griseoflavus* (Rodentia, Cricetidae). *Zeitchrift für Säugetierkunde* **59:** 14–20.

SUPPORTING INFORMATION

Additional Supporting Information may be found online in the supporting information tab for this article:

Figure S1. Bayesian 50% majority rule consensus tree obtained by means of partitioned analysis of the mitochondrial dataset (i.e. *mt-cyb*, ND3 and control region).
Figure S2. Bayesian 50% majority rule consensus tree obtained by means of partitioned analysis of nuclear dataset (i.e. IRBP, RAG1).
Figure S3. (A) Dorsal skull shape representations of the differences between the valid species (*Graomys chacoensis*, *Graomys griseoflavus*, and *Graomys domorum*) (dotted lines) and the holotypes of species whose taxonomic status is still debatable (*Graomys edithae*, *Graomys lockwoodi*, and *Graomys cachinus*) (continuous lines).
Figure S4. (A) Ventral skull shape representations of the differences between the valid species (*Graomys chacoensis*, *Graomys griseoflavus*, and *Graomys domorum*) (dotted lines) and the holotypes of species whose taxonomic status is still debatable (*Graomys edithae*, *Graomys lockwoodi*, and *Graomys cachinus*) (continuous lines).
Table S1. Vouchers used in the phylogeographical analysis of *mt-cyb* sequences.
Table S2. Primers used in molecular phylogenetic analyses.
Appendix S1. Vouchers and localities of the specimens used for the analysis of *mt-cyb* sequences (Fig. 1).
Appendix S2. List of specimens used for geometric morphometric analysis.